

# Chemical Kinetics of Methane Pyrolysis in Microwave Plasma at Atmospheric Pressure

Mirosław Dors · Helena Nowakowska · Mariusz Jasiński ·  
Jerzy Mizeraczyk

Received: 17 July 2013 / Accepted: 11 November 2013 / Published online: 24 November 2013  
© The Author(s) 2013. This article is published with open access at Springerlink.com

**Abstract** Results of chemical kinetics modeling in methane subjected to the microwave plasma at atmospheric pressure are presented in this paper. The reaction mechanism is based on the methane oxidation model without reactions involving nitrogen and oxygen. For the numerical calculations 0D and 1D models were created. 0D model uses Calorimetric Bomb Reactor whereas 1D model is constructed either as Plug Flow Reactor or as a chain of Plug Flow Reactor and Calorimetric Bomb Reactor. Both models explain experimental results and show the most important reactions responsible for the methane conversion and production of  $H_2$ ,  $C_2H_2$ ,  $C_2H_4$  and  $C_2H_6$  detected in the experiment. Main conclusion is that the chemical reactions in our experiment proceed by a thermal process and the products can be defined by considering thermodynamic equilibrium. Temperature characterizing the methane pyrolysis is 1,500–2,000 K, but plasma temperature is in the range of 4,000–5,700 K, which means that methane pyrolysis process is occurring outside the plasma region in the swirl gas flowing around the plasma.

**Keywords** Pyrolysis · Modeling · Methane · Microwave plasma

## Introduction

Microwave discharges at atmospheric pressure are efficient sources of reactive plasma, which can be employed for gas processing such as decomposition of volatile organic compounds, purification of noble gases, or hydrogen production from hydrocarbons, e.g. methane [1, 2]. The microwave plasma source (MPS) developed in our lab [3–6] is an

---

M. Dors (✉) · H. Nowakowska · M. Jasiński · J. Mizeraczyk  
Centre for Plasma and Laser Engineering, Institute of Fluid-Flow Machinery, Polish Academy  
of Sciences, Fiszerza 14, 80-231 Gdańsk, Poland  
e-mail: mdors@imp.gda.pl

J. Mizeraczyk  
Department of Marine Electronics, Gdynia Maritime University, Morska 83, 81-225 Gdynia, Poland

efficient apparatus for hydrogen production via hydrocarbons conversion. Although the presented MPS draws a parallel to other known atmospheric pressure microwave discharges such as a microwave torch [7] or a surfaguide-produced surface-wave discharge [8], which is also a waveguide-based one, it also draws some significant distinctions. As opposed to the plasma torch, where a nozzle is an important field-shaping element, our MPS is nozzleless, and the plasma is not created at the tip of the nozzle but in the reduced-height section region extending a few centimeters above and below it. The plasma region has greater diameter than that in both aforementioned discharges, where it is up to several millimeters. Obtaining plasma diameter up to 36 mm in gases used in our experiment without plasma contraction and filamentation, which is expected for typical surface-wave discharges [8, 9], is possible due to the high flow rate of the gas. In our MPS, the plasma region resembles rather an elongated flame than a regular plasma column. Its length weakly depends on microwave power, which is a behavior similar to that of torches and different from that of surface-wave discharges. Our preliminary theoretical study suggests that in this type of discharge the plasma is sustained by an electromagnetic wave. However, because the wave-shaping region is relatively long comparing to the plasma length, a pure mode cannot develop. A full description, either experimental or theoretical, of this type of high-flow microwave discharge has not been performed yet. All modeling of the MPS was limited to the physics of formation and changes in electrical field during the MPS operation [10].

In this paper we present the chemical kinetics modeling related to methane pyrolysis in the MPS. Experimental results were compared with the calculated ones. A set of 48 chemical reactions used in the model is presented in Table 1. It is based on the so called “Leeds methane oxidation mechanism” [11, 12]. In spite the fact that we observed soot formation in the experiment, we did not include the mechanism for its formation in the table. The problem of the soot formation has been studied experimentally and numerically for over 30 years and still is a challenge [13–16]. The important steps in soot formation from gas-phase hydrocarbons are believed to be formation of the first aromatic ring, formation of polycyclic aromatic hydrocarbons (PAHs), soot inception, and subsequently soot growth. In our case the path leading to soot formation starts from formation of acetylene which is considered as the principal intermediate species on the reaction path to the first benzene ring. However, due to the complexity of PAHs reactions we resigned from including them in our models.

In the model we did not include electron reactions either. From results presented by Nowakowska et al. in [17] it appears that in our discharge the reduced electric field  $E/N$  is of the 1 Td order and then electrons lose more than 90 % of their energy in inelastic collisions (for vibrational excitations) so their energy is too low to cause direct dissociation and ionization of gas molecules.

Numerical simulations of the plasma in methane were carried out using commercial software Chemical Work Bench, version 4 with extended database, by Kintech Ltd., Moscow, Russia. The basic assumption is that pressure  $P = \text{const}$ .

## Experimental Set-up

The MPS developed in our lab is presented schematically in Fig. 1. Details of the construction can be found in Jasinski et al. [6]. Briefly, this MPS, operating at atmospheric pressure and frequency 2.45 GHz, is based on a standard rectangular waveguide WR430 with a reduced-height section in the discharge region and two tapered sections on both

**Table 1** Chemical reactions used in the modeling of CH<sub>4</sub> pyrolysis in microwave plasma at atmospheric pressure

No	Reaction	$A$ (mol cm <sup>-3</sup> s <sup>-1</sup> )	$n$	$E$ (kcal mol <sup>-1</sup> )	Ref.
R1	H <sub>2</sub> + CH <sub>2</sub> (S) ⇌ CH <sub>3</sub> + H	1.2e-10	0	0	[20]
R2	CH <sub>4</sub> + C ⇌ CH + CH <sub>3</sub>	8.3e-11	0	24.015	[20]
R3	CH <sub>4</sub> + H ⇌ CH <sub>3</sub> + H <sub>2</sub>	2.19e-20	3	8.037	[21]
R4	CH <sub>4</sub> + CH ⇌ C <sub>2</sub> H <sub>4</sub> + H	5.0e-11	0	-0.396	[20]
R5	CH <sub>4</sub> + CH <sub>2</sub> ⇌ CH <sub>3</sub> + CH <sub>3</sub>	7.14e-12	0	10.038	[20]
R6	CH <sub>4</sub> + CH <sub>2</sub> (S) ⇌ CH <sub>3</sub> + CH <sub>3</sub>	1.16e-10	0	0	[22]
R7	CH <sub>4</sub> + C <sub>2</sub> H ⇌ CH <sub>3</sub> + C <sub>2</sub> H <sub>2</sub>	3.0e-12	0	0	[23]
R8	C <sub>2</sub> H <sub>2</sub> + C <sub>2</sub> H <sub>2</sub> ⇌ H <sub>2</sub> CCCCH + H	3.21e-15	0	57.84	[20]
R9	H <sub>2</sub> + C <sub>2</sub> H ⇌ C <sub>2</sub> H <sub>2</sub> + H	1.79e-11	0	2.165	[24]
R10	C + CH <sub>2</sub> ⇌ C <sub>2</sub> H + H	8.3e-11	0	0	[25]
R11	C + CH <sub>3</sub> ⇌ C <sub>2</sub> H <sub>2</sub> + H	8.3e-11	0	0	[26]
R12	H + H + M ⇌ H <sub>2</sub> + M	5.15e-30	-1	0	[26]
R13	H + H + H <sub>2</sub> ⇌ H <sub>2</sub> + H <sub>2</sub>	2.69e-31	-0.6	0	[20]
R14	H + CH ⇌ C + H <sub>2</sub>	1.39e-11	0	0	[20]
R15	H + CH <sub>2</sub> ⇌ CH + H <sub>2</sub>	1.0e-11	0	-1.78	[27]
R16	H + CH <sub>2</sub> (S) ⇌ CH <sub>2</sub> + H	3.32e-10	0	0	[20]
R17	H + CH <sub>3</sub> + M ⇌ CH <sub>4</sub> + M	3.88e-24	-1.8	0	[20]
R18	H + C <sub>2</sub> H <sub>3</sub> ⇌ C <sub>2</sub> H <sub>2</sub> + H <sub>2</sub>	2.0e-11	0	0	[20]
R19	CH <sub>3</sub> + CH <sub>3</sub> ⇌ C <sub>2</sub> H <sub>5</sub> + H	5.0e-11	0	13.51	[20]
R20	CH + CH <sub>2</sub> ⇌ C <sub>2</sub> H <sub>2</sub> + H	6.64e-11	0	0	[20]
R21	CH + CH <sub>3</sub> ⇌ C <sub>2</sub> H <sub>3</sub> + H	4.98e-11	0	0	[26]
R22	CH + C <sub>2</sub> H <sub>3</sub> ⇌ CH <sub>2</sub> + C <sub>2</sub> H <sub>2</sub>	8.3e-11	0	0	[26]
R23	CH <sub>2</sub> + CH <sub>2</sub> ⇌ C <sub>2</sub> H <sub>2</sub> + H <sub>2</sub>	2.0e-11	0	0.796	[26]
R24	CH <sub>2</sub> + CH <sub>2</sub> ⇌ C <sub>2</sub> H <sub>2</sub> + H + H	1.79e-10	0	0.796	[20]
R25	CH <sub>2</sub> + CH <sub>3</sub> ⇌ C <sub>2</sub> H <sub>4</sub> + H	7.0e-11	0	0	[20]
R26	CH <sub>2</sub> + C <sub>2</sub> H <sub>3</sub> ⇌ C <sub>2</sub> H <sub>2</sub> + CH <sub>3</sub>	3.0e-11	0	0	[20]
R27	CH <sub>2</sub> (S) + M ⇌ CH <sub>2</sub> + M	2.5e-11	0	0	[21]
R28	CH <sub>3</sub> + CH <sub>3</sub> + M ⇌ C <sub>2</sub> H <sub>6</sub> + M	1.0e-06	-7	2,763	[20]
R29	CH <sub>3</sub> + M ⇌ CH <sub>2</sub> + H + M	4.83e-08	0	90.61	[24]
R30	C <sub>2</sub> H + C <sub>2</sub> H <sub>3</sub> ⇌ C <sub>2</sub> H <sub>2</sub> + C <sub>2</sub> H <sub>2</sub>	3.15e-11	0	0	[20]
R31	H <sub>2</sub> CCCCH + M ⇌ C <sub>4</sub> H <sub>2</sub> + H + M	1.86e-08	0	46.51	[26]
R32	C <sub>2</sub> H <sub>2</sub> + H + M ⇌ C <sub>2</sub> H <sub>3</sub> + M	9.45e-30	0	1.47	[20]
R33	C <sub>2</sub> H <sub>2</sub> + CH ⇌ C <sub>2</sub> H + CH <sub>2</sub>	3.5e-10	0	-0.172	[20]
R34	C <sub>2</sub> H <sub>2</sub> + CH <sub>2</sub> ⇌ C <sub>3</sub> H <sub>4</sub>	2.0e-11	0	6.62	[20]
R35	C <sub>2</sub> H <sub>2</sub> + CH <sub>2</sub> (S) ⇌ H <sub>2</sub> CCCH + H	2.9e-10	0	0	[20]
R36	C <sub>2</sub> H <sub>2</sub> + C <sub>2</sub> H ⇌ C <sub>4</sub> H <sub>2</sub> + H	1.49e-10	0	0	[20]
R37	C <sub>2</sub> H <sub>2</sub> + M ⇌ C <sub>2</sub> H + H + M	1.89e-07	0	106.83	[20]
R38	C <sub>2</sub> H <sub>4</sub> + H ⇌ C <sub>2</sub> H <sub>3</sub> + H <sub>2</sub>	9.0e-10	0	14.9	[28]
R39	C <sub>2</sub> H <sub>4</sub> + H + M ⇌ C <sub>2</sub> H <sub>5</sub> + M	3.72e-29	0	0.755	[20]
R40	C <sub>2</sub> H <sub>4</sub> + CH ⇌ C <sub>3</sub> H <sub>4</sub> + H	2.19e-10	0	-0.344	[20]
R41	C <sub>2</sub> H <sub>4</sub> + CH <sub>2</sub> (S) ⇌ C <sub>3</sub> H <sub>4</sub>	1.6e-10	0	0	[20]
R42	C <sub>2</sub> H <sub>4</sub> + CH <sub>3</sub> ⇌ CH <sub>4</sub> + C <sub>2</sub> H <sub>3</sub>	6.91e-12	0	11.128	[20]

**Table 1** continued

No	Reaction	$A$ (mol cm <sup>-3</sup> s <sup>-1</sup> )	$n$	$E$ (kcal mol <sup>-1</sup> )	Ref.
R43	C <sub>2</sub> H <sub>4</sub> + M ⇌ C <sub>2</sub> H <sub>2</sub> + H <sub>2</sub> + M	1.65e-07	0	71.54	[20]
R44	C <sub>2</sub> H <sub>4</sub> + M ⇌ C <sub>2</sub> H <sub>3</sub> + H + M	1.26e-06	0	96.58	[20]
R45	C <sub>2</sub> H <sub>6</sub> + H ⇌ C <sub>2</sub> H <sub>5</sub> + H <sub>2</sub>	2.41e-15	0	7.411	[20]
R46	C <sub>2</sub> H <sub>6</sub> + CH ⇌ C <sub>2</sub> H <sub>4</sub> + CH <sub>3</sub>	1.79e-10	0	-0.263	[20]
R47	C <sub>2</sub> H <sub>6</sub> + CH <sub>2</sub> (S) ⇌ CH <sub>3</sub> + C <sub>2</sub> H <sub>5</sub>	3.98e-10	0	0	[20]
R48	C <sub>2</sub> H <sub>6</sub> + CH <sub>3</sub> ⇌ C <sub>2</sub> H <sub>5</sub> + CH <sub>4</sub>	2.51e-31	6	6.046	[23]

Reaction rate constant  $k$  follows Arrhenius formula:  $k(T) = AT^n \exp(E/RT)$

sides. The reduction of the height enables to obtain greater electric field intensity in the discharge region, and the tapered sections ensure a smooth transition between the sections of different heights. A movable short circuit (a microwave plunger) is a means of tuning. The discharge takes place in a fused silica tube that is placed in a metallic tube. Both tubes penetrate through the wider walls of the reduced-height section. The inner diameter of the discharge tube is 26 mm and the plasma column diameter is about 20 mm. Methane is delivered to the discharge region in the form of swirl with a flow rate of 50 dm<sup>3</sup>/min. Microwave power absorbed by the plasma is 2, 3 and 4 kW.

## 0D Model

### Model Description

For the 0D modeling of chemical kinetics we used Calorimetric Bomb Reactor (CBR) model with complete energy balance. The chemical composition and temperature evolution in the CBR are described on a self-consistent base using following equations:

- mass conservation equation for each component:

$$\rho \cdot \frac{dY_i}{dt} = \frac{\mu_i}{N_a} \cdot W_i \quad (1)$$

- energy conservation law:

$$\rho \cdot \frac{dh}{dt} = Q \quad (2)$$

- equation of state:

$$c_p \cdot \frac{dT}{dt} = - \sum_{i=1}^N \frac{h_i \cdot W_i \cdot \mu_i}{\rho \cdot N_a} + \frac{Q}{P} \quad (3)$$

where  $\rho$  is density,  $\mu_i$ —molecular weight of component,  $n$ —number of components,  $Y_i = \rho_i/\rho$ —mass fraction of component  $i$ ;  $W_i$ —chemical production rate of the component  $i$ ;  $Q$ —volume density of the external heat sources;  $N_a$ —Avogadro number;  $T$ —gas temperature.

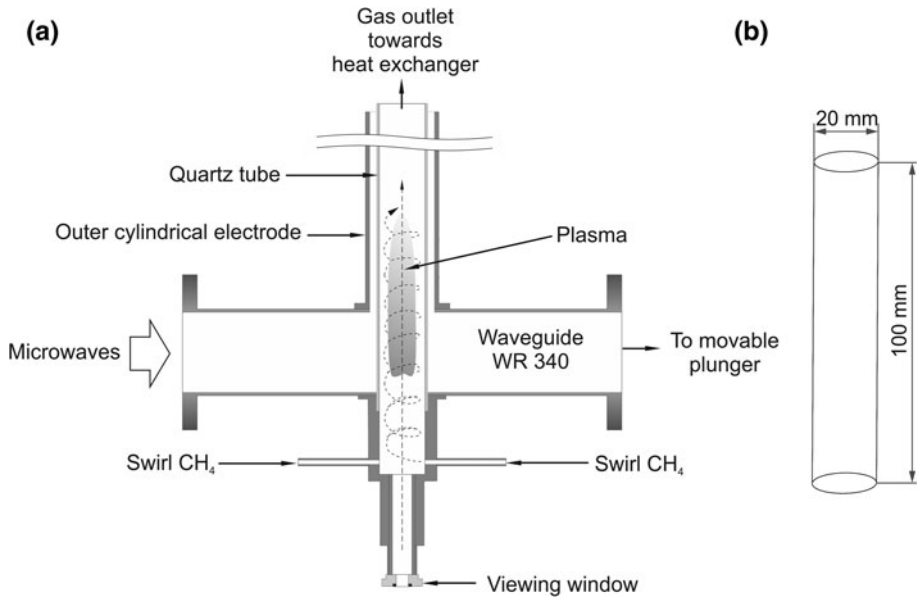


**Fig. 1** Schematic view of the experimental high-flow microwave plasma source (a) and 1D model representation (b)

Total enthalpy of each component  $h_i$  can be written in the form:

$$h_i = h_i^o + \int_{T_0}^T C_{pi} \cdot dT \tag{4}$$

where  $h_i^o$ —formation enthalpy of the  $i$ -th component at the reference temperature;  $C_{pi}$ —thermal capacity at a constant pressure;  $c_p$  is the mass-weighted mean specific heat:

$$c_p = \sum_{i=1}^N Y_i \cdot c_{pi} \tag{5}$$

In our model we assume that plasma is represented as a gas of high temperature and constant pressure. Calculations were made for initial temperatures ranging from 1,000 to 5,000 K with 100 K step and for residence time up to 1 s. Both, temperature and residence time cover much wider range than in the experiment. As shown by Jasinski et al. [6] the microwave plasma temperature in CH<sub>4</sub> is between 4,000 and 5,700 K, whereas residence time in the volume of plasma represented by the cylinder seen in Fig. 1b and resulting from the gas flow rate of 50 dm<sup>3</sup>/min is 0.037 s.

**Results**

Concentrations of all species included in the model can be presented as a function of temperature and time. Of the 20 species modeled only CH<sub>4</sub>, as a substrate, and 4 products, i.e. H<sub>2</sub>, C<sub>2</sub>H<sub>2</sub>, C<sub>2</sub>H<sub>4</sub> and C<sub>2</sub>H<sub>6</sub>, reach concentrations in experimentally measurable range. The final concentrations depend very much on the initial gas temperature. In Fig. 2 it is

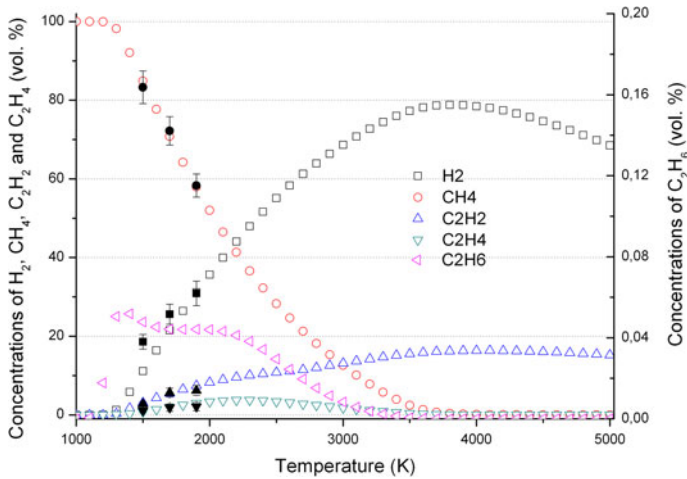


**Fig. 2** Concentrations of main species calculated using CBR model at residence time  $t = 1$  s. Experimental concentrations of  $\text{CH}_4$  (Circle),  $\text{H}_2$  (Square),  $\text{C}_2\text{H}_2$  (Triangle) and  $\text{C}_2\text{H}_4$  (Inverted Triangle) matching to calculated temperatures 1500 K, 1700 K and 1900 K are marked

seen that methane concentration starts decreasing at 1,200 K and reaches almost zero at 4,000 K. At this temperature hydrogen concentration is at maximum of 78.8 %. Further heating results in decomposition of molecular hydrogen into atoms.

Acetylene achieves the highest concentration of 16.4 % at 4,000 K and then slowly drops down. Concentration of  $\text{C}_2\text{H}_4$  grows to 3.8 % at 2,200 K and decreases to almost zero at 4,000 K. As for the  $\text{C}_2\text{H}_6$ , it is quickly produced to the maximum of 0.052 %, then drops down to 0.044 % at 1,700 K and remains constant up to 2,000 K. At higher temperature ethylene is decomposed completely.

Comparison with experimental results marked in Fig. 2 shows good agreement at initial temperatures of 1,500, 1,700 and 1,900 K. Those 3 sets of results matched at specific temperatures correspond to the experimentally used microwave power of 2, 3 and 4 kW, respectively. However, it must be pointed out that this agreement of numerical and experimental results was found only at 1 s, which corresponds not to residence time in plasma region (0.037 s) but rather to the total residence time in the system, i.e. from the introduction of the gas into the reactor to the sampling port.

In our simulations we used the CBR model with complete energy balance which means that during the chemical reactions temperature of the gas is changing and there are no heat losses due to radiation. This is well seen in Fig. 3 showing also kinetics of  $\text{CH}_4$  and products of its conversion when initial gas temperature is 1,800 K. The temperature drops in 1 s to 1,340 K due to transpiring reactions. The temperature drop means that overall process is endothermic.

Significant changes in concentrations of  $\text{CH}_4$  and main products start from 20  $\mu\text{s}$ . During 1 s methane decreases and hydrogen increases almost linearly, whereas acetylene reaches plateau at 0.1 s. Ethylene and ethane are characterized by the first peak at 0.2 ms followed by a slow decrease to the minimum at 22 ms and then their concentrations increase again.

Since the residence time in the assumed cylinder of plasma and resulting from the experimental gas flow is 37 ms the experimentally obtained concentrations of  $\text{H}_2$ ,  $\text{CH}_4$ ,

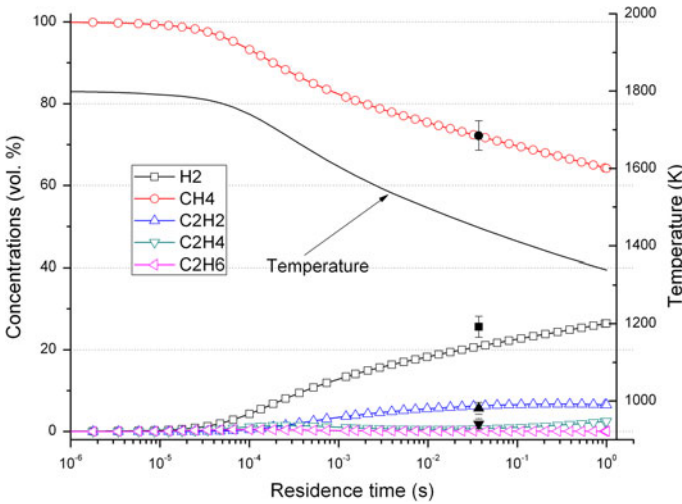


**Fig. 3** Concentrations of main species and gas temperature calculated using CBR model at the initial plasma temperature 1,800 K. Experimental concentrations of CH<sub>4</sub> (Circle), H<sub>2</sub> (Square), C<sub>2</sub>H<sub>2</sub> (Triangle) and C<sub>2</sub>H<sub>4</sub> (Inverted Triangle) are marked at residence time  $t = 0.037$  s

C<sub>2</sub>H<sub>2</sub> and C<sub>2</sub>H<sub>4</sub> are marked in Fig. 3 at this time. As seen, most compounds match relatively well to the calculations except for hydrogen concentration which is predicted to be lower than measured.

### 1D Model

#### Model Description

Microwave plasma formed in our MPS can be represented simply by a cylinder filled homogeneously with mixture of gases (Fig. 1b). It is assumed that the diameter and length of the cylinder is 2 and 10 cm, respectively, according to experimental data.

Chemical reactions and flow parameters evolution in the Plug Flow Reactor (PFR) can be described by the set of conservation laws equations of chemical hydrodynamics. These equations for steady state conditions in the reactor can be written in the following form:

- mass conservation equation:

$$\frac{d}{dx}(\rho \cdot u \cdot s) = 0 \tag{6}$$

- momentum conservation law:

$$u \cdot \frac{du}{dx} = -\frac{1}{\rho} \cdot \frac{dP}{dx} \tag{7}$$

- energy conservation law:

$$\rho \cdot u \frac{d}{dx} \left( \sum_i h_i \cdot Y_i + \frac{u^2}{2} \right) = Q \quad (8)$$

- mass conservation equations for each component:

$$u \cdot \frac{dY_i}{dx} = \frac{W_i}{\rho} \quad (9)$$

where  $x$ ,  $u$ ,  $s$ ,  $P$ —position along the reactor, velocity, cross sectional area and pressure of the gas flow, respectively. In this work it is assumed that pressure is constant in the PFR and there are no heat losses. The system (7)–(10) uses ideal gas law:

$$P = \rho \cdot R \cdot T \cdot \sum_{i=1}^n \frac{Y_i}{\mu_i} \quad (10)$$

where  $R$ —gas constant.

Total chemical reaction rate for each component can be written in the following form:

$$W_i = \sum_{j=1}^{j=M_i} \zeta_j^i \cdot k_j^i \cdot \prod_{k=1}^{k=B_j} \frac{\rho}{\mu_k} \cdot N_a \cdot Y_k \quad (11)$$

where  $M_i$ —number of chemical reactions which effect the concentration of the component  $i$ ;  $\zeta_j^i$ —number of the molecules generated or eliminated in the reaction  $i$ ;  $k_j^i$ —rate coefficient of chemical reaction  $j$ ;  $B_j^i$ —number of components which take part in the reaction  $j$  for component  $i$ .

## Results

Concentrations of methane and the main products obtained from the PFR model are presented in Fig. 4 as a function of plasma length at initial temperature of 2,000 K. At such a temperature experimental results match quite well the calculated values. Concentration profiles of all main compounds are similar to those obtained from the CBR model, i.e. decrease of  $\text{CH}_4$ , increase of  $\text{H}_2$ , increase of  $\text{C}_2\text{H}_2$  with the plateau, and maxima in concentrations of  $\text{C}_2\text{H}_4$  and  $\text{C}_2\text{H}_6$ . It must be pointed out that matching experimental and calculated values concerns the tip of the plasma cylindrical model. Temperature at that locations is much lower than initial temperature, but still far from the experimental one. In real conditions gas composition was diagnosed far away from the plasma when gas was cooled rapidly down to about 300 K using heat exchanger.

## 1D Model with Post-Plasma Quenching

In the experiment [6] gas composition analysis was carried out not along the microwave plasma or at its tip but far away, where processed gas was cold enough to be transported with PTFE tubes to the FTIR spectrometer and gas chromatograph. Cooling of the gas exiting the plasma was performed using an extensive heat exchanger placed 60 cm from



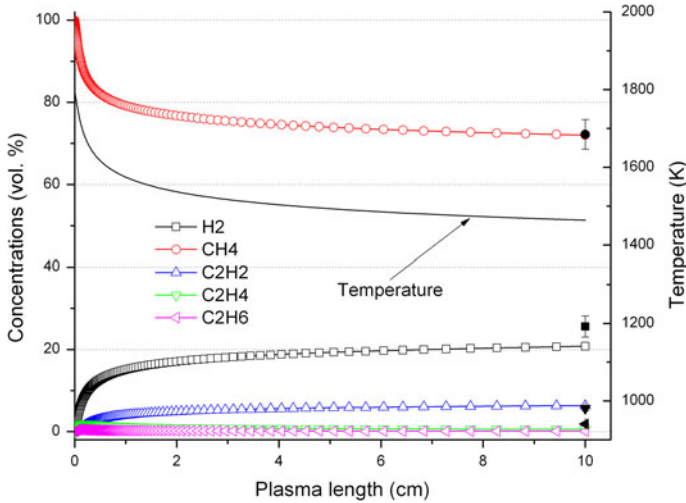


**Fig. 4** Concentrations of main species and gas temperature calculated using PFR model at the initial plasma temperature 1,800 K. Experimental concentrations of CH<sub>4</sub> (Circle), H<sub>2</sub> (Square), C<sub>2</sub>H<sub>2</sub> (Traingle) and C<sub>2</sub>H<sub>4</sub> (Inverted Traingle) are marked at the plasma tip

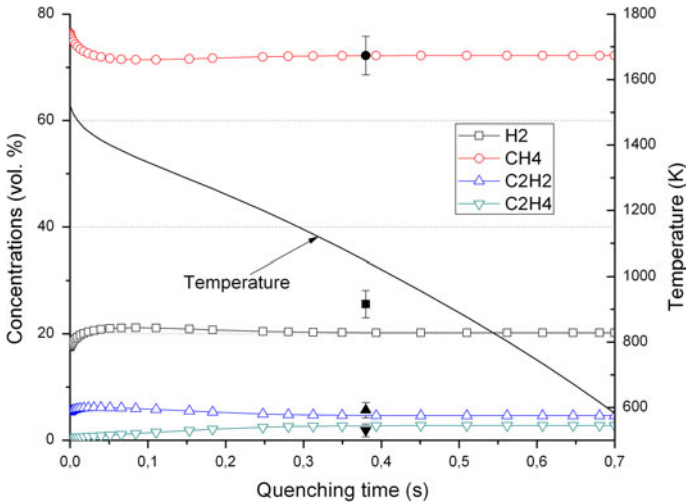


**Fig. 5** Concentrations of main species and gas temperature calculated using PFR with CBR model at the initial plasma temperature 1,800 K. Experimental concentrations of CH<sub>4</sub> (Circle), H<sub>2</sub> (Square), C<sub>2</sub>H<sub>2</sub> (Traingle) and C<sub>2</sub>H<sub>4</sub> (Inverted Traingle) are marked at quenching time  $t_q = 0.38$  s

the plasma tip. The quenching time, i.e. time in which gas is cooled down on its way from the plasma tip through the heat exchanger, at the gas flow of 50 dm<sup>3</sup>/min through the tube cross section, is 0.38 s. Thus, we modified the model of chemical kinetics by adding CBR (0D) after PFR (1D) which simulates gas temperature drop from initial 1,800 K down to 600 K in 0.7 s.

Simulated quenching reactions change the gas composition as seen in Fig. 5. In the case of methane and hydrogen, quenching reactions stabilize their concentrations relatively quickly, i.e. in about 0.5 s. Their further changes are insignificant. Small amount of acetylene is formed in the first 20 ms and then decomposed. Concentration of ethylene increases for about 0.35 s and then reaches plateau. Ethane is decomposed to very small concentration below our experimental detection limit, so it is not presented in Fig. 5.

Experimental results concerning  $\text{CH}_4$ ,  $\text{C}_2\text{H}_2$  and  $\text{C}_2\text{H}_4$  match well to the calculated values. Only  $\text{H}_2$  concentration is higher than predicted by the model. Taking into account the fact that methane is the only source of hydrogen in the model, we can explain the higher concentration of hydrogen measured in the experiment as a result of small amount of water vapor entering somehow the plasma region and operating as a source of additional portion of hydrogen. Evidence for that could be the imbalance of inlet hydrogen to the outlet which is 2 %.

## Discussion

Reaction mechanism used in the presented modeling was prepared from much larger mechanism by thorough reduction of less important reactions. Thus, all 48 reactions presented in the Table 1 are important. Removing even one reaction will have significant impact on the results of the modeling. Here we discuss the flux of C and H atoms in the proposed mechanism and contribution of reactions into decomposition of methane and formation of by-products.

Formation of H-containing radicals starts from  $\text{CH}_4$  and ends on  $\text{C}_3\text{H}_4$  and  $\text{H}_2\text{CCCCH}$ . Their final concentrations are very small, i.e. tens of ppm and ppb, respectively. However, they are important, in particular  $\text{H}_2\text{CCCCH}$ , for the formation of soot, which was observed in the experiment. The majority of H atoms transforms into  $\text{H}_2$ . Consequent measurable products are  $\text{C}_2\text{H}_4$  and  $\text{C}_2\text{H}_2$ . Other species are short-living intermediates.

Exactly the same sequence of radicals formation concerns the flux of C atoms, which is obvious since methane is the only substrate in the system. In that case  $\text{C}_2\text{H}$  radical is essential in the system. The C radical is neither the main nor final by-product of reactions, which means that it is not directly responsible for the soot formation. In the course of the mechanism preparation a reaction of  $\text{C}_2$  formation ( $2\text{C} + \text{M} \rightleftharpoons \text{C}_2 + \text{M}$ ) was added since  $\text{C}_2$  was detected spectroscopically in the experiment [6]. However, formation of  $\text{C}_2$  in the model and its contribution to C flux was so insignificant that finally we removed it from the mechanism.

Main reactions contributing to methane conversion and hydrogen production are presented in Figs. 6 and 7. Since contribution of reactions is varying in time, the presented state is at 37 ms, which is the experimental time used for comparing measured and calculated concentrations.

Thermally activated dissociation of the first C–H bond in  $\text{CH}_4$  molecule (R17) starts the chain of reactions. H atoms originated from that reaction attack  $\text{CH}_4$  causing formation of  $\text{H}_2$  (R3). This is the main reaction producing 74.6 % of  $\text{H}_2$ . Three other reactions contributing to the process of  $\text{H}_2$  formation are R45, R43 and R38. Their contributions are 10.8, 7.1 and 6.8 %, respectively.

The same reaction R3 is also the main one responsible for the decomposition of 71.5 % of  $\text{CH}_4$ . The second important reaction is R17 converting 29.3 % of  $\text{CH}_4$ . At the same time in two reactions, R48 and R42, large part of methane, i.e. 31 %, is restored.

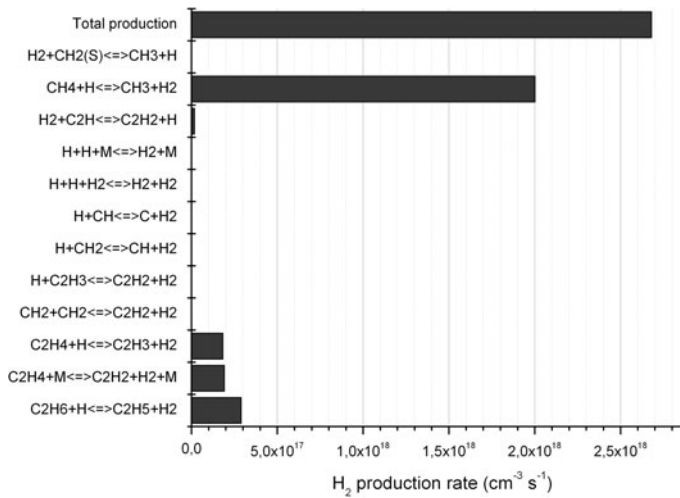


Fig. 6 Contribution of reactions producing H<sub>2</sub>

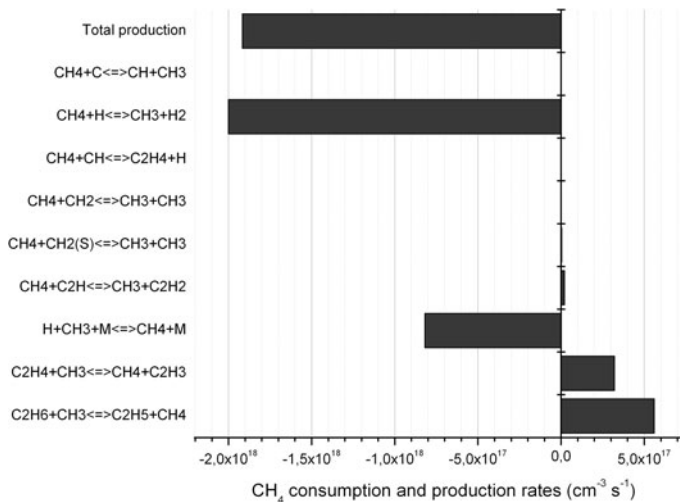
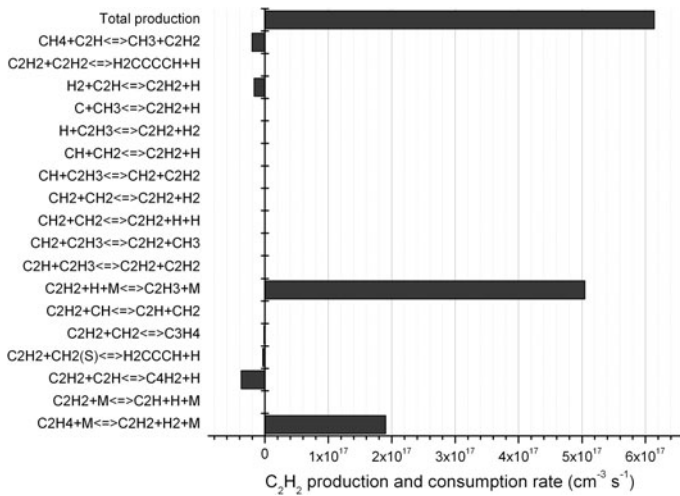


Fig. 7 Contribution of reactions decomposing and restoring CH<sub>4</sub>

As seen in Fig. 8 acetylene is involved in many reactions but is mainly produced by dehydrogenation of C<sub>2</sub>H<sub>4</sub> in direct reaction R43 and indirectly through C<sub>2</sub>H<sub>3</sub> radical in reaction R32. As for ethylene (Fig. 9), it is formed in one reaction R39 but decomposed in 3 reactions working also as sources of acetylene (R43) and restoring methane (R42).

Comparing to plasma chemistry reviewed by Lee et al. [18] reactions paths predicted by our model are typical for thermally activated ones. However, dehydrogenation of ethane leading to ethylene and acetylene is not based on Kassel mechanism [19] in which primary ethane is produced from CH<sub>4</sub> and CH<sub>2</sub>, not from CH<sub>3</sub>, and the final dehydrogenation product is atomic carbon. In our case dehydrogenation stops on C<sub>2</sub>H<sub>2</sub> which is further converted to soot precursors. This is, on the other hand, the pathway typical for methane combustion model [12].



**Fig. 8** Contribution of reactions involving C<sub>2</sub>H<sub>2</sub>

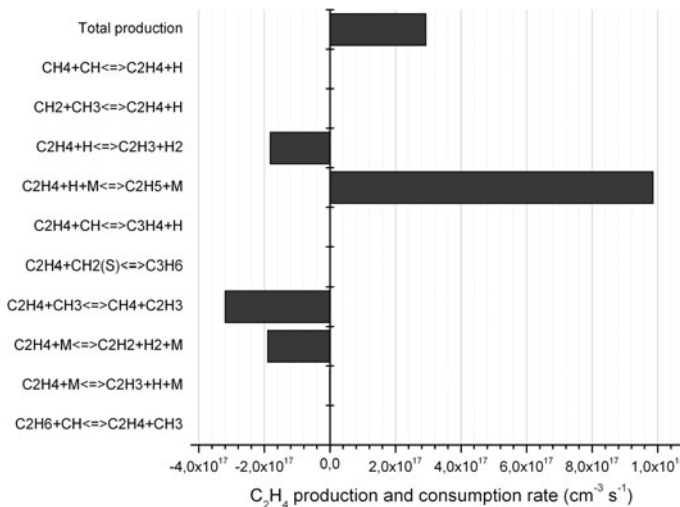


**Fig. 9** Contribution of reactions involving C<sub>2</sub>H<sub>4</sub>

One can notice that temperature characterizing the methane pyrolysis in our models is 1,500–2,000 K whereas temperature of plasma is 4,000–5,700 K [6]. This discrepancy means that the process is not occurring in the plasma region but in the swirl gas flowing around the plasma. Thus, in the experimental conditions just after introducing methane into the quartz tube the plasma operates as a heating source with a very small gas exchange towards the swirl and back. An evidence for that was observed as carbon black deposited on the quartz tube in the form of swirl below the plasma (negative values of distance in Fig. 10). If the methane is processed in the plasma then deposition of carbon soot should start above the point of plasma formation (marked as “0” in Fig. 10). Unfortunately, we cannot perform carbon balance due to the deposition of the carbon black inside the whole

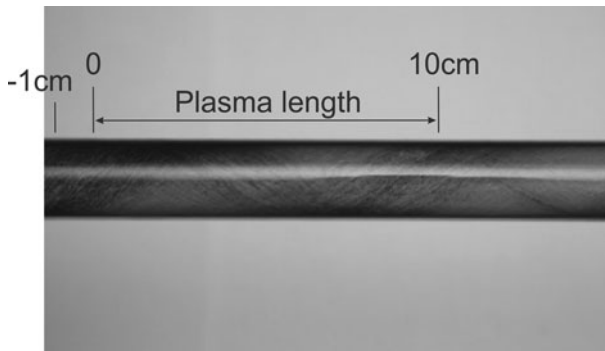


**Fig. 10** Visualization of the swirl: quartz tube covered with the soot after plasma processing of methane system starting from the beginning of the quartz tube to the gas sampling port (just before gas composition diagnostics).

## Summary

Results of chemical kinetics modeling in methane subjected to the microwave plasma at atmospheric pressure are presented in this report. The reaction mechanism is based on the methane oxidation model developed by the group from Leeds, UK. For the numerical calculations 0D and 1D models were created. 0D model uses Calorimetric Bomb Reactor whereas 1D model is constructed either as Plug Flow Reactor or as a chain of Plug Flow Reactor and Calorimetric Bomb Reactor. Commercial software Chemical Workbench, Version 4, (Kintech Laboratory, Moscow, Russia) with extended database has been used for the modeling. Both models explain experimental results and show most important reactions responsible for the methane conversion and production of compounds detected in the experiment. Main products of methane pyrolysis measured and predicted by the model are  $H_2$ ,  $C_2H_2$  and  $C_2H_4$ .

The main conclusion is that chemical kinetics in our experiment is controlled by thermal process and the products can be defined by considering thermodynamic equilibrium. Temperature characterizing the methane pyrolysis is 1,500–2,000 K which means that the process is not occurring in the plasma region where the temperature is 4,000–5,700 K but in the swirl gas flowing around the plasma.

**Acknowledgments** This research has been supported by the Polish Ministry of Science and Higher Education (MNiSW) under the program PB 2595/B/T02/2008/35.

**Open Access** This article is distributed under the terms of the Creative Commons Attribution License which permits any use, distribution, and reproduction in any medium, provided the original author(s) and the source are credited.

## References

1. Uhm HS, Hong YC, Shin DH (2006) A microwave plasma torch and its application. *Plasma Sources Sci Technol* 15:S26–S34
2. Kabouzi Y, Moisan M, Rostaing JC, Trassy C, Keroack D, Zakrzewski Z (2003) Abatement of per-fluorinated compounds using microwave plasmas at atmospheric pressure. *J Appl Phys* 93:9483–9496

- Jasiński M, Dors M, Nowakowska H, Mizeraczyk J (2008) Hydrogen production using various microwave plasma sources. *Chem Listy* 102:1332–1337
- Jasiński M, Dors M, Mizeraczyk J (2008) Production of hydrogen via methane reforming using atmospheric pressure microwave plasma. *J Power Sources* 181:41–45
- Jasinski M, Dors M, Mizeraczyk J (2009) Destruction of Freon HFC-134a using a nozzleless microwave plasma source. *Plasma Chem Plasma Process* 29:363–372
- Jasiński M, Czykowski D, Hrycak B, Dors M, Mizeraczyk J (2013) Atmospheric pressure microwave plasma source for hydrogen production. *Int J Hydrogen Energy*. doi:10.1016/j.ijhydene.2013.05.105
- Moisan M, Sauve G, Zakrzewski Z, Hubert J (1994) An atmospheric pressure waveguide-fed microwave plasma torch: the TIA design. *Plasma Sources Sci Technol* 3:584–592
- Moisan M, Zakrzewski Z (1995) Plasma sources using long linear microwave field applicators: main features, classification and modeling. *Plasma Sources Sci Technol* 4:379–397
- Kabouzi Y, Moisan M (2005) Pulsed microwave discharges sustained at atmospheric pressure: study of the contraction and filamentation phenomena. *IEEE Trans Plasma Sci* 33:292–293
- Nowakowska H, Jasiński M, Dębicki P, Mizeraczyk J (2011) Numerical analysis and optimization of power coupling efficiency in waveguide-based microwave plasma source. *IEEE Trans Plasma Sci* 39:1935–1941
- The Leeds methane oxidation mechanism, Version 1.5, <http://garfield.chem.elte.hu/Combustion/methane.htm>
- Hughes KJ, Turanyi T, Clague AR, Pilling MJ (2001) Development and testing of a comprehensive chemical mechanism for the oxidation of methane. *Int J Chem Kinet* 33:513–538
- Sirignano M, Kent J, D'Anna A (2013) Modeling formation and oxidation of soot in nonpremixed flames. *Energy Fuels* 27:2303–2315
- Valin S, Cances J, Castelli P, Thiery S, Dufour A, Boissonnet G, Spindler B (2009) Upgrading biomass pyrolysis gas by conversion of methane at high temperature: experiments and modeling. *Fuel* 88:834–842
- Slavinskaya NA, Frank P (2009) A modelling study of aromatic soot precursors formation in laminar methane and ethene flames. *Combust Flame* 156:1705–1722
- Skjøth-Rasmussen MS, Glarborg P, Østberg M, Johannessen JT, Livbjerg H, Jensen AD, Christensen TS (2004) Formation of polycyclic aromatic hydrocarbons and soot in fuel-rich oxidation of methane in a laminar flow reactor. *Combust Flame* 136:91–128
- Nowakowska H, Jasiński M, Mizeraczyk J (2010) Two-dimensional simulations of atmospheric pressure microwave discharge in methane, XX European conf. on the atomic and molecular physics of ionized gases, 13–17 July, Novi Sad, Serbia
- Lee DH, Kim K-T, Song Y-H, Kang WS, Jo S (2013) Mapping plasma chemistry in hydrocarbon fuel processing processes. *Plasma Chem Plasma Process* 33:249–269
- Kassel LS (1932) The thermal decomposition of CH<sub>4</sub>. *J Am Chem Soc* 54:3949–3961
- Baulch DL, Cobos CJ, Cox RA, Frank P, Hayman G, Just Th, Kerr JA, Murrells T, Pilling MJ, Troe J, Walker RW, Warnatz J (1994) Evaluated kinetic data for combustion modelling supplement I. *J Phys Chem Ref Data* 23:847–1033
- Glarborg P, Miller JA, Kee RJ (1986) Kinetic modeling and sensitivity analysis of nitrogen oxide formation in well-stirred reactors. *Combust Flame* 64:177–202
- Bohland T, Dobe S, Temps F, Wagner HG (1985) Kinetics of the reactions between CH<sub>2</sub>(X<sup>3</sup>B<sub>1</sub>)-radicals and saturated hydrocarbons in the temperature range 296 K ≤ T ≤ 707 K. *Ber Bunsenges Phys Chem* 89:1110–1116
- Langford AO, Petek H, Moore CB (1983) Collisional removal of CH<sub>2</sub>(<sup>1</sup>A<sub>1</sub>)—absolute rate constants for atomic and molecular collisional partners at 295 K. *J Chem Phys* 78:6650–6659
- Tsang W, Hampson RF (1986) Chemical kinetic database for combustion chemistry. I. Methane and related-compounds. *J Phys Chem Ref Data* 15:1087–1279
- Frank P, Bhaskaran KA, Just T (1986) High-temperature reactions of triplet methylene and ketene with radicals. *J Phys Chem* 90:2226–2231
- Miller JA, Bowman CT (1989) Mechanism and modeling of nitrogen chemistry in combustion. *Prog Energy Combust Sci* 15:287–338
- Becker KH, Engelhardt B, Wiesen P, Bayes KD (1989) Rate constants for CH(X<sup>2</sup>Π) reactions at low total pressures. *Chem Phys Lett* 154:342–348
- Warnatz J (1984) In: Gardiner WC Jr (ed) *Combustion chemistry*. Springer, New York